

Proximity nanovalve with large phase-tunable thermal conductance

E. Strambini,^{1, a)} F. S. Bergeret,^{2, 3, 4, b)} and F. Giazotto^{1, c)}

¹⁾NEST Istituto Nanoscienze-CNR and Scuola Normale Superiore, I-56127 Pisa, Italy

²⁾Centro de Física de Materiales (CFM-MPC), Centro Mixto CSIC-UPV/EHU, Manuel de Lardizabal 4, E-20018 San Sebastián, Spain

³⁾Donostia International Physics Center (DIPC), Manuel de Lardizabal 5, E-20018 San Sebastián, Spain

⁴⁾Institut für Physik, Carl von Ossietzky Universität, D-26111 Oldenburg, Germany

We propose a phase-controlled heat-flux quantum valve based on the proximity effect driven by a superconducting quantum interference proximity transistor (SQUIPT). Its operation relies on the phase-dependent quasiparticle density of states in the Josephson weak-link of the SQUIPT which controls thermal transport across the device. In a realistic Al/Cu-based setup the structure can provide efficient control of thermal current inducing temperature swings exceeding ~ 100 mK, and flux-to-temperature transfer coefficients up to ~ 500 mK/ Φ_0 below 100 mK. The nanovalve performances improve by lowering the bath temperature, making the proposed structure a promising building-block for the implementation of coherent caloritronic devices operating below 1 K.

Phase-dependent manipulation of heat in solid-state nanodevices is nowadays one of the major challenges of coherent caloritronics¹, and plays a key role in determining the physical properties of mesoscopic systems at low temperature. Toward this direction, the prototype for a heat interferometer has been recently realized with a superconducting quantum interference device (SQUID) where the modulation of the thermal current has been achieved thanks to the Josephson coupling^{2–5}. Yet, phase-dependent thermal transport has been also demonstrated in Andreev interferometers^{6–8} where the proximity effect in a normal metal affects its thermal conductance, and is controlled via a magnetic field.

Here we propose an alternative approach to control heat transport by envisioning a thermal nanovalve based on proximity effect but phase-controlled by a SQUIPT^{9–12}. Differing from SQUID-based and Andreev interferometers our device allows a drastic quenching of the thermal conductance which makes our proposal an efficient phase-tunable thermal nanovalve. Specifically, we expect an improvement of the temperature swing (up to ~ 100 mK) and a flux-to-temperature transfer function exceeding 500 mK/ Φ_0 at 100 mK.

A sketch for the proximity nanovalve is shown in Fig. 1(a) and consists of a SQUIPT composed by a superconducting (S) ring interrupted by a diffusive normal metal (N) wire of length L . We assume the wire transverse dimensions to be negligible in comparison to its length so that it can be considered as quasi-one-dimensional. Superconducting correlations are induced in the N wire owing to proximity effect from the S loop

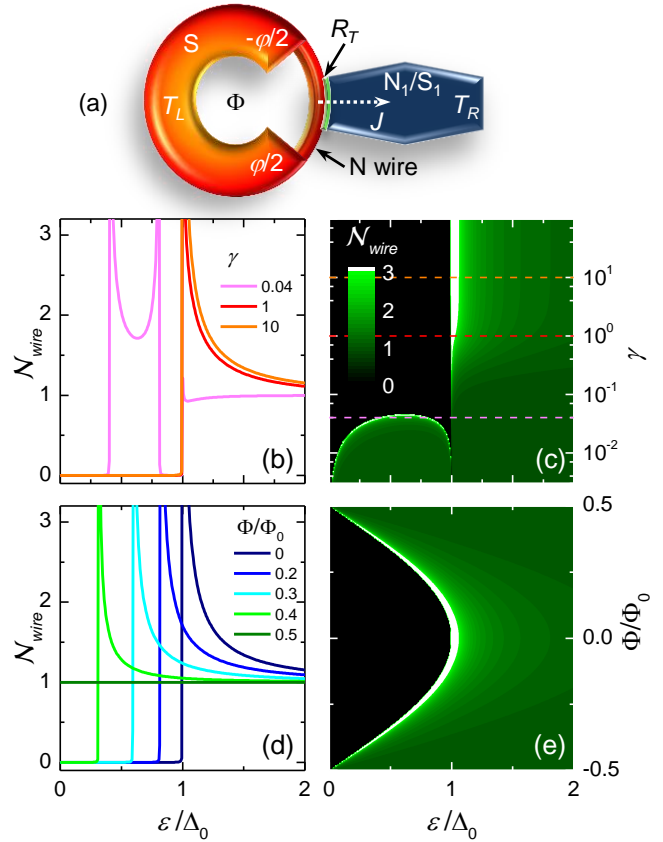


FIG. 1. (a) Sketch of the proximity nanovalve discussed in the text. J denotes the thermal current flowing through the structure. (b) N_{wire} vs energy ε calculated for a few values of γ at $\Phi = 0$. (c) Color plot of N_{wire} vs ε and γ at $\Phi = 0$. (d) N_{wire} vs ε calculated for $\gamma = 10$ at different values of Φ , and (e) corresponding color plot in ε and Φ . All the calculations were performed at zero temperature.

^{a)}Electronic mail: e.strambini@sns.it

^{b)}Electronic mail: sebastian.bergeret@ehu.es

^{c)}Electronic mail: f.giazotto@sns.it

which modifies the wire density of states (DoS)¹³. In addition, a normal metal (N_1) or a superconducting electrode (S_1) identical to S is tunnel-coupled to the middle of the wire through an insulating contact of negligible width respect to the wire length. R_T denotes the normal-state resistance of the junction. We assume the SN ring and the N_1 (or S_1) electrode to be in steady-state thermal equilibrium and to reside at different temperatures T_L and T_R , respectively, with $T_L \geq T_R$. The nanovalve is therefore only temperature biased. In the limit of negligible geometric inductance of the ring it follows that $\varphi = 2\pi\Phi/\Phi_0$, where φ is the phase difference across the SN boundaries, Φ is the applied magnetic flux through the loop, and $\Phi_0 = 2.067 \times 10^{-15}$ Wb is the flux quantum. The ring geometry allows to change φ which leads to the modification of the N-wire DoS¹⁴ and, in turn, a drastic modification of *thermal* transport through the device.

The DoS in the N wire (\mathcal{N}_{wire}) is given by $\mathcal{N}_{wire}(\varepsilon, x) = |\text{Re}[g^R(\varepsilon, x)]|$, where g_R is the normal retarded quasiclassical Green's function, ε is the energy, and x is the spatial coordinate along the wire. The function g^R can be obtained by solving the one-dimensional Usadel equation (we skip the supra index R)¹⁵

$$\hbar D \partial_x (\hat{g} \partial_x \hat{g}) + (\varepsilon + i\Gamma) [\hat{\tau}_z, \hat{g}] = 0, \quad (1)$$

where D is the wire diffusion coefficient, the parameter Γ accounts for the inelastic scattering rate within the relaxation time approximation^{16–19}, and $\hat{\tau}_z$ is the third Pauli matrix in the Nambu space. The Green's function \hat{g} is a matrix in this space with the form $\hat{g} = g\hat{\tau}_z + \hat{f}$, being \hat{f} the anomalous Green's function that is off-diagonal in Nambu space. The Usadel equation has to be complemented by the normalization condition $\hat{g}^2 = \hat{1}$, where $\hat{1}$ is the unit matrix. The SN interfaces are modeled by proper boundary conditions. If the SN interfaces have large contact resistance R_{SN} we use the Kupiyanov-Lukichev boundary conditions²⁰ $\hat{g} \partial_x \hat{g}|_{x=\pm L/2} = \pm \frac{1}{2R_{SN}\mathcal{A}\sigma} [\hat{g}_{\pm}, \hat{g}]$, where \mathcal{A} is cross sectional area of the SN interface, σ the conductance of the N-wire and \hat{g}_{\pm} are the Green's functions of the left and right S electrodes defined as $\hat{g}_{\pm} = g_s \hat{\tau}_3 + f_s [\cos(\varphi/2) i\tau_2 \pm \sin(\varphi/2) i\tau_1]$. Here, $g_s(\varepsilon) = \frac{\varepsilon + i\Gamma}{\sqrt{(\varepsilon + i\Gamma)^2 - \Delta^2}}$, $f_s(\varepsilon) = \frac{\Delta}{\sqrt{(\varepsilon + i\Gamma)^2 - \Delta^2}}$, Δ is the BCS temperature-dependent energy gap with critical temperature $T_c = (1.764 k_B)^{-1} \Delta_0$, Δ_0 is the zero-temperature order parameter and k_B is the Boltzmann constant. Furthermore, we neglect the suppression of the ring order parameter at the SN interfaces due to *inverse* proximity effect. This latter can be made negligible by making the wire cross section much smaller than that of the S loop^{9,21,22}. If the SN contact resistance is negligibly small one imposes the continuity of the Green's functions at the interface.

We first focus on the *short* junction limit (i.e., $E_{Th} = \hbar D/L^2 \gg \Delta_0$, where E_{Th} is the SNS junction Thouless energy). In this case the proximity effect can be maximized, and the performance of the nanovalve enhanced.

This limit can be practically met with a copper N wire ($D = 0.01$ m²/s) of 100 nm length and an aluminum S ring ($\Delta_0 = 200$ μ eV) for which $E_{Th} = 3.3 \Delta_0$. In such a case, the DoS in N can be obtained analytically:

$$\mathcal{N}_{wire} = \left| \text{Re} \left[\frac{\varepsilon - 2i\varepsilon_b g_s}{\sqrt{(\varepsilon - 2i\varepsilon_b g_s)^2 + [2\varepsilon_b f_s \cos(\frac{\pi\Phi}{\Phi_0})]^2}} \right] \right|, \quad (2)$$

where $\varepsilon_b = \hbar D/(2LR_{SN}\mathcal{A}\sigma) = \gamma E_{Th}$, and $\gamma \equiv R_N/R_{SN}$ quantifies the transmissivity of the SN contact²³.

Figure 1(b) and (c) show \mathcal{N}_{wire} vs energy ε for different γ values at $\Phi = 0$. A clear energy gap Δ_0 in the DoS is visible even for quite low interface transmissivity (down to $\gamma \sim 0.1$) while for smaller γ we observe the suppression of the minigap due to the weak coupling with S. Moreover, the minigap damping is bounded by the generation of a secondary gap appearing for $\varepsilon \lesssim \Delta_0$, similarly to what has been predicted in Ref.^{24,25}. In the following, unless differently stated, we will set $\Gamma = 10^{-4} \Delta_0$ and $\gamma = 10$, as estimated from realistic values of transparent Al/Cu SN interfaces²⁶. For this transmissivity the external magnetic flux Φ can efficiently modulate the minigap of the DoS in accordance to Eq. (2). Figure 1(d) and (e) show this modulation, where a clear quenching of the minigap is visible for $|\Phi| = \Phi_0/2$. This DoS modulation is the working principle of the present device and allows heat transport when the wire is in the normal state (i.e., for $|\Phi| = \Phi_0/2$) whereas it provides large thermal isolation when it is in the superconducting one. Full control over the heat current flowing through the device is one of the peculiar properties of this nanovalve that, differently from the other phase-coherent thermal modulators^{2–8}, allows an almost complete quenching of the heat flow. The thermal current (J) flowing from the SN ring to the $N_1(S_1)$ electrode [see Fig. 1(a)] can be written as²⁷ $J = \frac{2}{e^2 R_T} \int_0^\infty d\varepsilon \mathcal{N}_{wire}(\varepsilon, \Phi) \mathcal{N}(\varepsilon) \mathcal{F}(\varepsilon)$, where $\mathcal{N}(\varepsilon) = 1$ for N_1 , $\mathcal{N}(\varepsilon) = |\text{Re}[(\varepsilon + i\Gamma)/\sqrt{(\varepsilon + i\Gamma)^2 - \Delta^2}]|$ for S_1 , $\mathcal{F}(\varepsilon) = [f_0(\varepsilon, T_L) - f_0(\varepsilon, T_R)]$, $f_0(\varepsilon, T_{L,R}) = [1 + \exp(\varepsilon/k_B T_{L,R})]^{-1}$ is the Fermi-Dirac distribution function, and e is the electron charge. When the temperature difference between the SN ring and the $N_1(S_1)$ electrode is small, $\delta T \equiv T_L - T_R \ll T \equiv (T_L + T_R)/2$, we can define the thermal conductance in the linear-response regime, $\kappa \equiv J/\delta T$, which can be written as

$$\kappa = \frac{\alpha}{T^2} \int_0^\infty d\varepsilon \varepsilon^2 \mathcal{N}_{wire}(\varepsilon, \Phi) \mathcal{N}(\varepsilon) \text{sech}^2 \left(\frac{\varepsilon}{2k_B T} \right), \quad (3)$$

where $\alpha = (2e^2 k_B R_T)^{-1}$. For $T > T_c$, Eq. (3) reduces to $\kappa^N = \mathcal{L}_0 T/R_T$ (Wiedemann-Franz law) where $\mathcal{L}_0 = \pi^2 k_B^2/3e^2$ is the Lorenz number.

Figure 2(a) and (b) display the behavior of $\kappa(T)$ calculated for a few values of Φ , for a normal (N_1) and a superconducting (S_1) electrode, respectively. At low temperature ($T \lesssim 0.1 T_c$) a large suppression of κ can be achieved for $\Phi = 0$ (i.e., down to $10^{-4} \kappa^N$) due to the

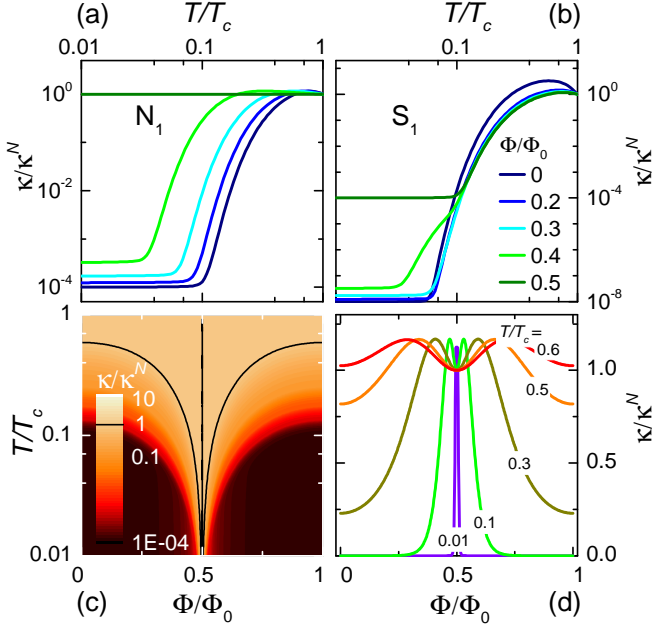


FIG. 2. Comparison between the nanovalve thermal conductance κ vs temperature T calculated for a N_1 , (a), and a S_1 , (b), electrode. (c) Color plot of κ calculated in (a) vs Φ and T and (d) cross sections of it at selected temperatures T .

presence of a S-like DoS in the wire which leads to a reduction of quasiparticles available for thermal transport, and which is only limited by the finite value of Γ . At fixed T , κ then gradually increases, as displayed in Fig. 2(c) and (d), eventually coinciding with κ^N by closing the minigap at $\Phi_0/2$. We emphasize that although a heat valve effect could be achieved as well by replacing the N_1 electrode with a superconductor S_1 [see Fig 2(b)], the performance of the resulting structure, apart a stronger quenching of κ at low T , worsen owing to the presence of the energy gap in S_1 which severely limits the heat current flow. For this reason in the following we will focus on the properties of the nanovalve implemented with a N_1 electrode. In order to obtain large κ modulations a tunnel contact between the N wire and N_1 is crucial. The presence of a *clean* metallic contact indeed leads to a drastic degradation of the superconducting-like properties of the N-wire due to *inverse* proximity effect⁸.

The heat valve efficiency of this setup can be quantified through the phase-dependent thermal conductance ratio (PTC) defined as: $\text{PTC}(T, \Phi) = [\kappa(T, \Phi) - \kappa(T, 0)]/\kappa(T, 0)$. As can be noticed in Fig. 3(a) and (c), where the PTC ratio is calculated vs T and Φ , respectively, the nanovalve can be highly efficient at temperatures below $\sim T_c/2$ with a PTC exceeding 100% for $T < 0.2T_c$, and saturating to Δ_0/Γ at $T \lesssim 0.1T_c$ for $\Phi = \Phi_0/2$, as shown in Fig. 3(b). Moreover, at low temperature, the thermal valve is more sensitive to the mag-

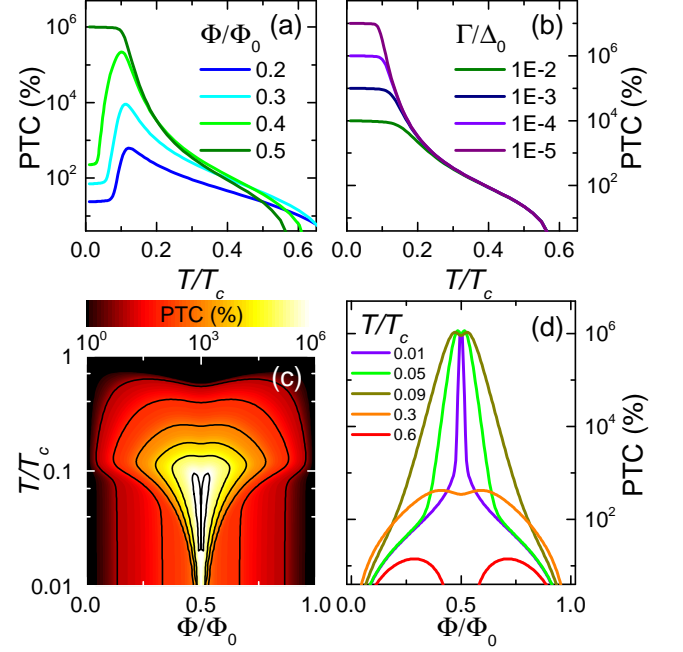


FIG. 3. Phase-dependent thermal conductance ratio (PTC) vs T calculated for few values of Φ , (a), and for a few values of Γ at $\Phi = \Phi_0/2$, (b). (c) PTC vs Φ and T . (d) Representative cross sections of panel (c) at selected temperatures T .

netic flux Φ , as demonstrated by the sharp open/close transitions appearing around $\sim \Phi_0/2$ in Fig. 3(d).

All the above results have been obtained from Eq. (2), which is valid in the limit of a short N-wire. In the case of an arbitrary length we have solved numerically the Usadel equation (1) in the N region^{28,29} to obtain the DoS in the middle of the wire and compute the thermal conductance κ from Eq. (3). The solutions are shown in Fig. 4 where the behavior of κ in T and Φ is displayed for different E_{Th} . At large E_{Th} the solutions converge to the analytical one (represented by the dashed lines) that well approximates κ for $E_{Th} \gtrsim \Delta_0$. Moreover, the general trend of κ in T and Φ is reproduced also for longer wires ($E_{Th} < \Delta_0$) with a damping of κ still three order of magnitude smaller than κ_N at low temperatures (i.e., for $T < 0.05T_c$), therefore ensuring full functionality of the thermal nanovalve even for $E_{Th} = 0.25\Delta_0$.

According to the above conditions the experimental realization of our thermal nanovalve can be easily achieved with conventional metals and standard lithographic techniques^{9–12}. Superconducting tunnel junctions additionally coupled to the SN ring and the N_1 electrode, serving either as heaters or thermometers, allow to change and monitor the quasiparticle temperature on both sides of the structure²⁷. We neglect here the contribution to thermal transport through these probes as they can provide nearly-ideal thermal isolation of the nanovalve electrodes.

Figure 5(a) shows the relevant model accounting for

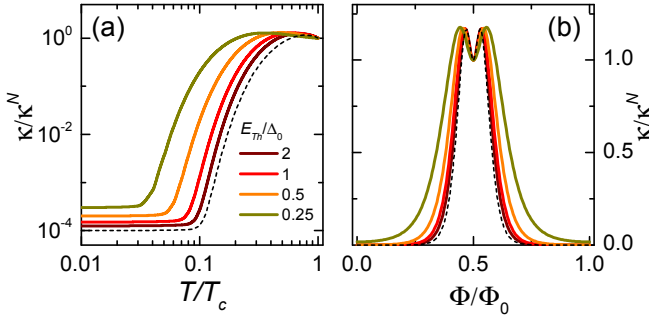


FIG. 4. Comparison between the nanovalve thermal conductance κ calculated from the solution of the Usadel equations for different E_{Th} (continuous lines) and in the *short* junction limit (dashed lines) vs T for $\Phi = 0$, (a), and vs Φ for $T = 0.1 T_c$, (b).

thermal transport in the device. Upon intentionally heating the SN ring at T_L the steady-state electron temperature T_R will depend on the heat exchange mechanisms occurring in N_1 . Below ~ 1 K, the energy relaxation mechanism in N_1 stems mainly from electron-acoustic phonon interaction²⁷, $J_{e-ph,R}(T_R, T_{ph}) = \Sigma V(T_R^n - T_{ph}^n)$, which allows heat exchange between quasiparticle and lattice phonons residing at T_{ph} . Above, Σ is the material-dependent electron-phonon coupling constant, V is the volume, and n is the characteristic exponent of the N_1 metal. In the model we neglect thermal transport mediated by photons^{30–32} as well as pure heat conduction by phonons³³. For any given T_{ph} and T_L , the steady-state $T_R(\Phi)$ is then obtained by solving the thermal balance equation $-J(T_L, T_R, \Phi) + J_{e-ph,R}(T_R, T_{ph}) = 0$. For the following calculations we assume an aluminum (Al) ring with $\Delta_0 = 200 \mu\text{eV}$, $\Gamma = 10^{-4} \Delta_0$, $R_T = 100 \text{ k}\Omega$, $V = 2 \times 10^{-20} \text{ m}^3$, $n = 6$ and $\Sigma = 4 \times 10^9 \text{ WK}^{-6} \text{ m}^{-3}$ as appropriate for an AlMn N_1 electrode^{1,5}. Furthermore, we assume the SNS junction to be in the *short* limit which, according to the above discussions, properly describes the framework of a realistic nanovalve^{10–12}.

Phase-dependent control of thermal current through the nanovalve is demonstrated by the strong modulation of $T_R(\Phi)$ displayed in Fig. 5(b) for different values of T_L at $T_{ph} = 20 \text{ mK}$. In particular, it can exceed 100 mK at $T_L = 200 \text{ mK}$. The high response of the heat valve, quantified by the flux-to-heat current transfer coefficient ($\mathcal{T} \equiv \partial J / \partial \Phi$)^{2,3}, is demonstrated in Fig. 5(c) where \mathcal{T} is plotted for the same T_L values of panel (b). In particular, \mathcal{T} obtains values as large as $\sim 500 \text{ mK}/\Phi_0$ at 20 mK and for $T_L \lesssim 0.1 T_c$, and it keeps increasing at lower T_L , as shown in Fig. 5(e). Moreover, to quantify the visibility of temperature T_R modulation induced by the magnetic flux we define the parameter $\nu = \delta T_R / T_{ph}$, where $\delta T_R = \max[T_R(\Phi)] - \min[T_R(\Phi)]$. A full characterization of ν as a function of T_L and T_{ph} is shown in Fig. 5(d). According to the calculations, a sizeable T_R modulation is still visible ($\nu > 10\%$) up to 300 mK of

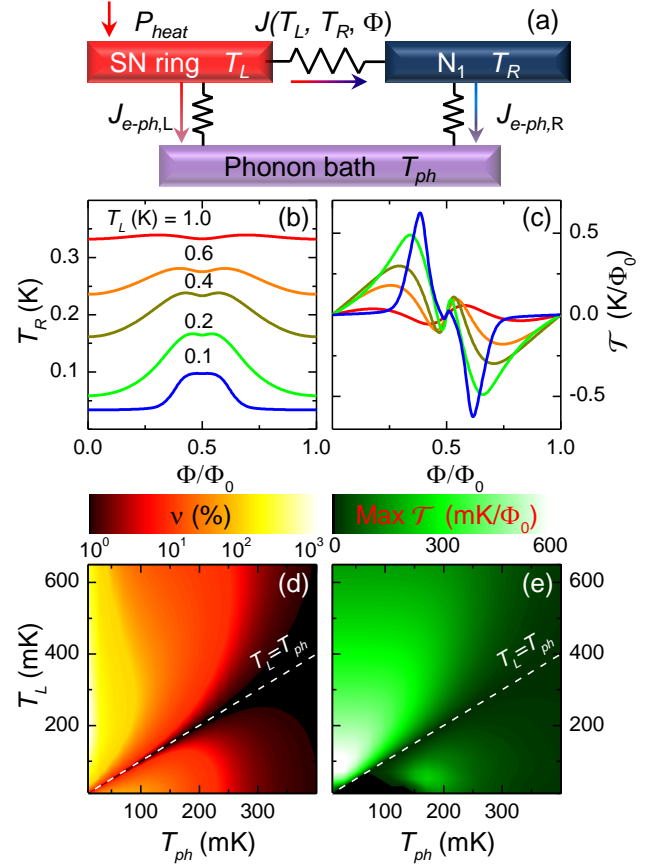


FIG. 5. (a) Sketch of the thermal model accounting for heat transport in the proximity nanovalve. $J_{e-ph,L(R)}$ represents the heat current flowing between quasiparticles and lattice phonons residing at T_{ph} in the left(right) electrode, whereas P_{heat} denotes the power injected into the SN ring in order to impose a quasiparticle temperature T_L . The arrows indicate the direction of heat currents for $T_L > T_R > T_{ph}$. (b) Temperature T_R vs Φ calculated for selected T_L assuming $T_{ph} = 20 \text{ mK}$. (c) Flux-to-temperature transfer function \mathcal{T} vs Φ calculated from the data in panel (b). Color plots of the thermal visibility ν , (d), and the maximal transfer function, (e), achievable with the proximity nanovalve vs T_{ph} and T_L .

bath temperature and, differing from the SQUID-based thermal modulator³, the visibility is strongly enhanced at lower T_{ph} exceeding 1000% at 20 mK. Notably, the proximity nanovalve demonstrates good performance also for the temperature regime where $T_L < T_{ph}$, as shown by the high efficiency and large transfer functions visible in the regions below the white dashed lines of panels (d) and (e).

In summary, we have proposed a thermal nanovalve based on the SQUIPT technology which is able to efficiently conduct or isolate heat depending on the magnitude of an applied magnetic flux. Under experimentally accessible conditions the device can provide full phase control of the thermal conductance, which is unique at cryogenic temperatures. Standard nanolithographic

techniques and conventional metals provide a straightforward route towards the implementation of this thermal nanovalve.

We acknowledge P. Virtanen for fruitful discussions. The work of E.S. and F.G. was partially funded by the European Research Council under the European Union's Seventh Framework Programme (FP7/2007-2013)/ERC grant agreement No. 615187-COMANCHE, and by the Marie Curie Initial Training Action (ITN) Q-NET 264034. The work of F.S.B. was supported by the Spanish Ministry of Economy and Competitiveness under Project No. FIS2011-28851-C02-02 the Basque Government under UPV/EHU Project No. IT-756-13.

- ¹M. J. Martínez-Pérez, P. Solinas, and F. Giazotto, *J. Low Temp. Phys.* **175**, 813 (2014).
- ²F. Giazotto and M. J. Martínez-Pérez, *Nature* **492**, 401 (2012).
- ³F. Giazotto and M. J. Martínez-Pérez, *Appl. Phys. Lett.* **101**, 102601 (2012).
- ⁴M. J. Martínez-Pérez and F. Giazotto, *Appl. Phys. Lett.* **102**, 092602 (2013).
- ⁵M. J. Martínez-Pérez and F. Giazotto, *Nat. Commun.* **5** (2014), 10.1038/ncomms4579.
- ⁶J. Eom, C.-J. Chien, and V. Chandrasekhar, *Phys. Rev. Lett.* **81**, 437 (1998).
- ⁷D. A. Dikin, S. Jung, and V. Chandrasekhar, *Phys. Rev. B* **65**, 012511 (2001).
- ⁸E. V. Bezuglyi and V. Vinokur, *Phys. Rev. Lett.* **91**, 137002 (2003).
- ⁹F. Giazotto, J. T. Peltonen, M. Meschke, and J. P. Pekola, *Nat. Phys.* **6**, 254 (2010).
- ¹⁰M. Meschke, J. T. Peltonen, J. P. Pekola, and F. Giazotto, *Phys. Rev. B* **84**, 214514 (2011).
- ¹¹R. N. Jabdaraghi, M. Meschke, and J. P. Pekola, *Appl. Phys. Lett.* **104**, 082601 (2014).
- ¹²A. Ronzani, C. Altimiras, and F. Giazotto, *arXiv:1404.4206 [cond-mat]* (2014).
- ¹³S. Guéron, H. Pothier, N. O. Birge, D. Esteve, and M. H. Devoret, *Phys. Rev. Lett.* **77**, 3025 (1996).
- ¹⁴F. Zhou, P. Charlat, B. Spivak, and B. Pannetier, *J. Low Temp. Phys.* **110**, 841 (1998).
- ¹⁵K. D. Usadel, *Phys. Rev. Lett.* **25**, 507 (1970).
- ¹⁶R. C. Dynes, J. P. Garno, G. B. Hertel, and T. P. Orlando, *Phys. Rev. Lett.* **53**, 2437 (1984).
- ¹⁷J. P. Pekola, T. T. Heikkilä, A. M. Savin, J. T. Flyktman, F. Giazotto, and F. W. J. Hekking, *Phys. Rev. Lett.* **92**, 056804 (2004).
- ¹⁸J. P. Pekola, V. F. Maisi, S. Kafanov, N. Chekurov, A. Kemppinen, Y. A. Pashkin, O.-P. Saira, M. Möttönen, and J. S. Tsai, *Phys. Rev. Lett.* **105**, 026803 (2010).
- ¹⁹O.-P. Saira, A. Kemppinen, V. F. Maisi, and J. P. Pekola, *Phys. Rev. B* **85**, 012504 (2012).
- ²⁰M. Y. Pekriyanov and V. F. Lukichev, *Sov. Phys. JETP* **67**, 1163 (1988).
- ²¹H. le Sueur, P. Joyez, H. Pothier, C. Urbina, and D. Esteve, *Phys. Rev. Lett.* **100**, 197002 (2008).
- ²²J. C. Hammer, J. C. Cuevas, F. S. Bergeret, and W. Belzig, *Phys. Rev. B* **76**, 064514 (2007).
- ²³F. Giazotto and F. S. Bergeret, *Appl. Phys. Lett.* **102**, 162406 (2013).
- ²⁴A. Levchenko, *Phys. Rev. B* **77**, 180503 (2008).
- ²⁵J. Reutlinger, L. Glazman, Y. V. Nazarov, and W. Belzig, *Phys. Rev. Lett.* **112**, 067001 (2014).
- ²⁶H. Courtois, M. Meschke, J. T. Peltonen, and J. P. Pekola, *Phys. Rev. Lett.* **101**, 067002 (2008).
- ²⁷F. Giazotto, T. T. Heikkilä, A. Luukanen, A. M. Savin, and J. P. Pekola, *Rev. Mod. Phys.* **78**, 217 (2006).
- ²⁸P. Virtanen and T. T. Heikkilä, *Appl. Phys. A* **89**, 625 (2007).
- ²⁹P. Virtanen, “Quasiclassical equations on a 1d network,” (2009), source code for the solution of the Usadel equation available at <http://ltdl.tkk.fi/~theory/usadel1/>.
- ³⁰D. R. Schmidt, R. J. Schoelkopf, and A. N. Cleland, *Phys. Rev. Lett.* **93**, 045901 (2004).
- ³¹M. Meschke, W. Guichard, and J. P. Pekola, *Nature* **444**, 187 (2006).
- ³²L. M. A. Pascal, H. Courtois, and F. W. J. Hekking, *Phys. Rev. B* **83**, 125113 (2011).
- ³³K. Maki and A. Griffin, *Phys. Rev. Lett.* **15**, 921 (1965).